PCCP

Accepted Manuscript

This is an *Accepted Manuscript*, which has been through the Royal Society of Chemistry peer review process and has been accepted for publication.

Accepted Manuscripts are published online shortly after acceptance, before technical editing, formatting and proof reading. Using this free service, authors can make their results available to the community, in citable form, before we publish the edited article. We will replace this *Accepted Manuscript* with the edited and formatted *Advance Article* as soon as it is available.

You can find more information about *Accepted Manuscripts* in the **Information for Authors**.

Please note that technical editing may introduce minor changes to the text and/or graphics, which may alter content. The journal's standard **Terms & Conditions** and the **Ethical guidelines** still apply. In no event shall the Royal Society of Chemistry be held responsible for any errors or omissions in this *Accepted Manuscript* or any consequences arising from the use of any information it contains.

Physical Chemistry Chemical Physics Accepted Manuscript

PCCP

ARTICLE

Growth of Cu particles on Cu$_2$O truncated octahedron: tuning of the Cu content for efficient glucose sensing

Gang Wang, Hong Sun, Lu Ding, Gang Zhou and Zhong-Sheng Wang*

A simple and versatile hydrothermal method is developed to synthesize Cu-Cu$_2$O, in which Cu particles grow on the surface of Cu$_2$O truncated octahedron. Through the reduction of Cu^{2+} by glucose in an alkaline solution, Cu$_2$O truncated octahedron is quickly formed via a kinetic control process, and then Cu particles selectively nucleate on the high-energy (110) facets of Cu$_2$O, generating a heterostructure. The amount of Cu in the sample is successfully tuned by varying the reaction temperature. Compared to Cu$_2$O, the hybrid Cu-Cu$_2$O architecture shows superior electrocatalytic performance for glucose oxidation due to the synergistic effect between more electrocatalytic active but less conutive Cu$_2$O and more conductive but less electrocatalytic active Cu. By tuning the content of Cu in the heterostructure, the highest electrocatalytic activity is achieved at the molar ratio Cu/Cu$_2$O of 0.83.

1. Introduction

Glucose sensing is of considerable importance in diagnosis and management of diabetes mellitus as well as in process monitoring and control of food industries.[1,2] It is hence necessary to achieve sensitive, reliable, and low-cost glucose sensors. Previous glucose sensors usually involve the use of enzymes such as glucose oxidase (GOx).[3] However, because of the poor stability of enzymes and degradation of GOx activity during the immobilization process, such enzyme-based sensors usually suffer from unsatisfactory reproducibility and insufficient long-term stability.[4] Therefore, increasing attempts have been undertaken to develop electrochemical non-enzymatic glucose biosensors.

Many studies on the direct electrochemical oxidation of glucose have used a large number of electrocatalysts such as transition metals and their oxides (Au, Pt, Co, Cu, Ni, Co$_3$O$_4$, NiO, Fe$_2$O$_3$, WO$_3$, RuO$_2$, Cu$_2$O, etc.).[5-7] Among them, Cu$_2$O is relatively inexpensive, less toxic, biocompatible, and appropriate for numerous applications. Moreover, it was reported by Xie et al. in 1991 that Cu$_2$O can function as a highly efficient electrocatalyst for glucose oxidation resulting from the redox couple of Cu(III)/Cu(II) in the alkaline medium.[8] Thus, there have been extensive investigations on Cu$_2$O-based materials as electrode materials for constructing non-enzyme biosensors.[9-11] It was reported that Cu$_2$O octahedron had good stability and high catalytic activity.[12, 13] In addition, a recent study revealed that Cu$_2$O octahedron was highly conductive compared to Cu$_2$O cubic and rhombic dodecahedron.[14] Owing

to these merits, Cu$_2$O octahedron is a promising candidate for the electrochemical oxidation of glucose.[15]

It has been noticed that involving a second phase (e.g. graphene, carbon nanotubes, carbon spheres) in electrode materials can greatly enhance the electrocatalytic activity.[16-19] The second phase can increase the surface-area-to-volume ratio, porosity, and charge-transfer kinetics. Carbon quantum dots and Au as a decorating phase to Cu$_2$O are also found to benefit the glucose oxidation.[15,20] Recently, Cu(0) has been found to act as a co-catalyst of Cu$_2$O.[21,22] The Cu-Cu$_2$O hybrid shows advantages over Cu$_2$O because the presence of Cu can enhance the electrochemical active area of the electrode due to the improved conductivity. Furthermore, Cu as an inorganic decorating phase can lead to good dispersibility in an aqueous solution, which is challenging for conventional carbon materials.[23] While the composite with a Cu core and a partial oxide Cu$_2$O shell has been reported,[24,25] growth of Cu particles on Cu$_2$O has rarely been reported. Although several methods, such as polyol method and liquid phase method,[21,22,26] have been used for preparation of Cu-Cu$_2$O composite, facile synthesis of well-defined Cu-Cu$_2$O hybrid with precise component control remains challenging. Furthermore, there have been few studies on the function of Cu in the Cu-Cu$_2$O hybrid catalyst.

In this work, Cu-Cu$_2$O composites with well-defined structures have been prepared through a one-step hydrothermal method using glucose as a green reductant, which is mild, fast, and environmentally friendly. Under the reaction condition, Cu$_2$O truncated octahedron is quickly formed and the Cu particles are subsequently formed on the high-energy (110) planes of Cu$_2$O. The activity of Cu-Cu$_2$O deposited fluorine doped tin oxide (FTO) electrode is found to be copper content dependent. Owing to the synergistic effect between electrocatalytic active Cu$_2$O and conductive Cu, the

Department of Chemistry, Laboratory of Advanced Materials, iChEM (Collaborative Innovation Center of Chemistry for Energy Materials), Fudan University, 2205 Songhu Road, Shanghai 200438, P. R. China. E-mail: zs.wang@fudan.edu.cn
† Electronic Supplementary Information (ESI) available. See DOI: 10.1039/x0xx00000x

Cu-Cu$_2$O heterostructure shows a much higher electrocatalytic activity on glucose sensing than both Cu$_2$O and Cu.

2. Experimental

2.1. Materials

Cu(NO$_3$)$_2$·3H$_2$O, NaOH, KCl, tartaric acid, chitosan (CHT), isopropanol, dopamine (DA), uric acid (UA), ascorbic acid (AA), fructose, lactose and sucrose were purchased from Sinopharm Chemical Reagent Co., Ltd (Shanghai, China). Glucose (C$_6$H$_{12}$O$_6$), hydrazine and K$_3$Fe(CN)$_6$ were purchased from Aladding. All of the chemicals are analytical grade reagents and used as received.

2.2. Synthesis of Cu-Cu$_2$O truncated octahedron

In a typical synthesis, 0.1801 g (1 mmol) glucose, 4 mL of 1 M NaOH solution and 2.5 mL of 0.2 M Cu(NO$_3$)$_2$ solution were added to 40 mL of deionized water in order under magnetic stirring to form a deep blue transparent solution. This solution was continuously stirred for 5 min. Then, the solution was transferred to a 100 mL Teflon-lined autoclave and allowed to react for 6 h at 60 - 120 ^{o}C. After the reaction is completed, it is cooled to RT naturally outside the oven. The claret product was centrifuged followed by washing with degased water and ethanol. The resultant product was dried at 60 ^{o}C and stored in a glass vial for further use. The samples synthesized at 60, 80 100 and 120 ^{o}C for 6 h are denoted as Cu-Cu$_2$O(T), where T is the reaction temperature. For example, Cu-Cu$_2$O(60) represents the sample prepared at 60 ^{o}C.

2.3. Synthesis of truncated Cu$_2$O octahedron

The synthetic procedures of truncated Cu$_2$O octahedron was identical to those of Cu-Cu$_2$O truncated octahedron at 60 ^{o}C except the hydrothermal reaction time reduced from 6 to 1 h.

2.4. Synthesis of truncated Cu

Firstly, 0.6000 g (4 mmol) tartaric acid was dissolved in 20 mL 1 M NaOH solution in a 50 mL round bottom flask under magnetic stirring. Then, 1 mL of 0.2 M Cu(NO$_3$)$_2$ solution was added to the above solution under stirring. The mixed solution was then heated at 50 ^{o}C under magnetic stirring at 500 rpm for 10 min. Hydrazine (0.068 mL, 50 wt%) was quickly injected into the heated solution using pipet. The resulting solution was left undisturbed for 30 min after 30 s stirring. Subsequently, the reaction was removed from the oil bath and allowed to cool to RT. The product was centrifuged followed by washing with degased water and ethanol to remove the excess tartrate. The resultant product was dried at 50 ^{o}C and stored in a glass vial for further use.

2.5. Preparation of modified electrodes

The fluorine doped tin oxide (FTO, 14 Ω per square, 2.0 mm thick, Nippon Sheet Glass Co., Ltd., Japan) was washed carefully with isopropanol, ethanol and deionized water under ultrasonication for 30 min each. The geometric active area of the modified FTO electrode was confined to 0.3 × 0.3 cm^2 with a polyimide tape. Then, 20 μL of 4 mg mL^{-1} suspension of Cu-Cu$_2$O was drop cast onto the FTO followed by drop casting 2 μL of 1 mg mL^{-1} CHT solution to obtain the CHT/Cu-Cu$_2$O/FTO electrode. The modified electrodes were dried in air prior to measurements. For comparison, CHT/Cu$_2$O/FTO and CHT/Cu/FTO electrodes were also prepared with the similar process. The use of CHT is to make the film being firmly adhered to the substrate. The thickness of these electrodes was 3.5 ± 0.3 μm.

2.6. Apparatus and measurements

The X-ray diffraction (XRD) profile was recorded on an X-ray powder diffractometer (D8 Advance, Bruker) with Cu Kα radiation (λ = 0.154 nm). The morphology of the sample was examined with field emission scanning electron microscopy (FESEM, S-4800, Hitachi). The component content in Cu-Cu$_2$O was detected by inductively coupled plasma-atomic emission spectroscopy (ICP-AES, Thermo Electron Corp. Adv. ER/S). The microstructure was characterized with high-resolution transmission electron microscopy (HRTEM, JEM-2100F, JEOL). All the electrochemical measurements were performed on an electrochemical workstation (CHI 660D) in a three-electrode system, at a scan rate of 50 mV s^{-1}. The catalyst deposited FTO with a geometric active area of 0.09 cm^2 was employed as the working electrode, with a Pt wire as the counter electrode and an Ag/AgCl (3 M KCl) electrode as the reference electrode. The bare FTO as the working electrode was used to scan the background.

The cyclic voltammogram (CV) was recorded in 0.1 M NaOH solution by scanning the potential in the range between 0 and 0.6 V. The electrochemical impedance spectroscopy (EIS) was scanned at a potential of 0.24 V in the frequency range of 10^6-0.01 Hz with an amplitude of 10 mV using 5 mM K$_3$Fe(CN)$_6$ containing 0.1 M KCl as the supporting electrolyte. Amperometric analysis was carried out in 0.1 M NaOH solution at a fixed potential.

3. Results and discussion

3.1. Cu-Cu$_2$O truncated octahedron prepared by glucose reduction

The Cu-Cu$_2$O heterostructures were synthesized by simply mixing glucose, deionized water, NaOH and Cu(NO$_3$)$_2$·3H$_2$O in order followed by heating the reaction system at different temperatures for 6 h. Once the Cu(NO$_3$)$_2$·3H$_2$O was added to the above reaction system, a transparent solution was formed. The deep blue colour of the mixture indicates that the copper ions turn into [Cu(OH)$_4$]$^{2-}$ complex instead of forming precipitation before being reduced to form Cu$_2$O. The formation of the [Cu(OH)$_4$]$^{2-}$ complex is more favourable due to the high concentration of OH$^-$ anions in solution.[27] Through

the over-reduction of $Cu(NO_3)_2$ at temperature from 60 to 120 ^{o}C for 6 h, the deep blue transparent solution generated a claret precipitate ultimately.

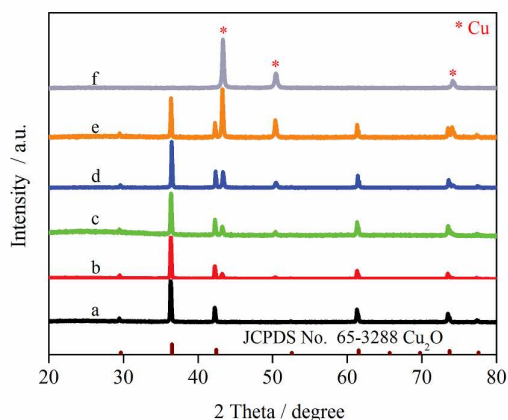Fig. 1 XRD patterns of (a) Cu_2O, (b) Cu-Cu_2O(60), (c) Cu-Cu_2O(80), (d) Cu-Cu_2O(100), (e) Cu-Cu_2O(120), and (f) Cu. The star shows diffraction peaks of cubic copper (JCPDS No. 04-0836).

The as-prepared powders were subjected to XRD analysis. When the temperature was low and the reaction time was short (at 60 ^{o}C for 1 h), the product was pure cubic Cu_2O, as revealed by the XRD pattern in Fig. 1 (trace a). The observed XRD peaks at 29.6^o, 36.5 ^{o}, 42.4 ^{o}, 61.5 ^{o}, 73.7 ^{o} and 77.5 ^{o} correspond to the (110), (111), (200), (220), (311) and (222) crystal planes of Cu_2O (JCPDS NO. 65-3288). However, the XRD patterns of the samples prepared at various temperatures for 6 h show two suits of characteristic peaks (Fig. 1, traces b-e), indicating their hybrid nature. Besides the XRD peaks for Cu_2O, the peaks at 43.3^o, 50.4^o and 74.1^o are indexed to (111), (200) and (220) crystal planes of copper (JCPDS No. 04-0836). The well-resolved and strong diffraction peaks evidence good crystallinity of these samples. The intensities of copper (111), (200) and (220) peaks increase with temperature, suggesting an increased content of copper with temperature. The molar ratios of Cu/Cu_2O carefully measured with ICP are 0.22, 0.44, 0.83, and 3.38 for Cu-Cu_2O(60), Cu-Cu_2O(80), Cu-Cu_2O(100), and Cu-Cu_2O(120), respectively, as summarized in Table S1. We also synthesized Cu particles, and its XRD pattern is also shown in Fig. 1 (trace f) for comparison.
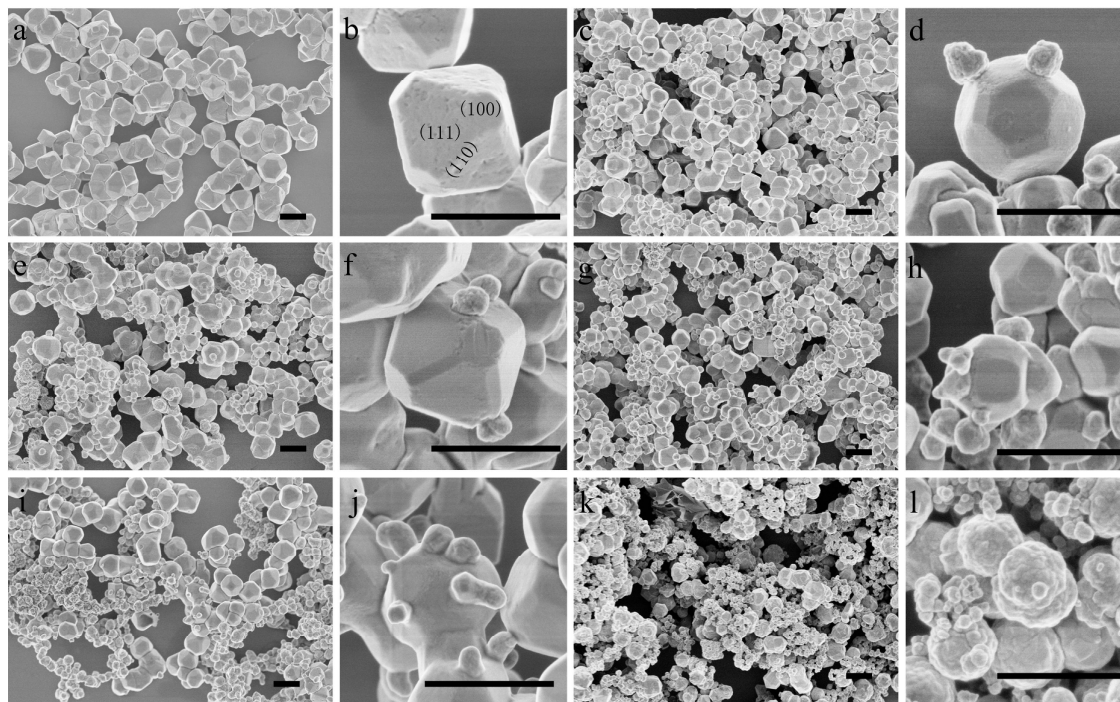

Fig. 2 FESEM images of (a, b) Cu_2O, (c, d) Cu-Cu_2O(60), (e, f) Cu-Cu_2O(80), (g, h) Cu-Cu_2O(100), (i, j) Cu-Cu_2O(120), and (k, l) Cu. The scale bars represent 1 μm.

Fig. 2 shows the SEM images of Cu_2O, Cu-Cu_2O and Cu. Fig. 2a shows the morphology of Cu_2O synthesized at 60 ^{o}C for 1 h. The as-prepared Cu_2O (~1000 nm) is a typical truncated octahedron, which is enclosed by eight (111) facets, six (100) facets and twelve (110) facets (Fig. 2b). When the reaction time was extended to 6 h at the same temperature (60 ^{o}C), smaller particles (300 nm) were formed and distributed on the surface of truncated octahedron. According to the XRD result, the larger truncated octahedron may be Cu_2O and the smaller

particle may be Cu, which will be further discussed in the following paragraph. When the reaction was kept at temperatures from 60 to 120 ^{o}C for 6 h, the obtained samples showed a similar hierarchical structure composed of smaller particles (300 nm) on larger particles (750-1350 nm). The number of Cu particles attached to one Cu_2O octahedron increased with reaction temperature (Fig. 2 d, f, h, j). This indicates that higher temperature provide driving force to

overcome energy barrier for the nucleation of Cu, thus offering more nucleation sites on one truncated octahedron.

To further investigate the component of such a heterostructure, Cu-Cu$_2$O(60) as a representative was subjected to TEM analysis (Fig. 3). The insert TEM image in Fig. 3a shows a typical Cu-Cu$_2$O hybrid structure. It is clear that smaller particles (*ca.* 300 nm) are located on the larger polyhedron (*ca.* 1300 nm), in conformity with the SEM images. Three parts are chosen to analyze the crystal structure. The red circle highlights the interface between the smaller particle and larger truncated octahedron (insert of Fig. 3a). The HRTEM image reveals that the smaller particle shows clear (111) lattice fringe of Cu, while (200) lattice fringe of Cu$_2$O is observed on the edge of another part. It is concluded that the larger octahedron is Cu$_2$O and the smaller particle is Cu. Another two parts are respectively selected from the smaller particle (blue circle) and the larger truncated octahedron (green circle) for

the selected area electron diffraction (SAED) analysis. Fig. 3b shows the SAED pattern of the green circle, which demonstrates the typical characteristics of a single-crystal structure.[28,29] The diffraction spots can be indexed to the [001] zone axis of Cu$_2$O. The corresponding HRTEM micrograph shows the facets vertical to the [001] zone. The interplanar spacing is measured to be 0.301 nm, corresponding to the (110) plane of a cubic Cu$_2$O (Fig. 3c). The SAED (Fig. 3d) of the smaller particle (blue circle) recorded along the [002] zone axis confirms the single-crystal structure of Cu. Fig. 2e shows the HRTEM image of the marked area (blue circle in Fig. 3a). The typical fringe spacing is determined to be 0.208 nm, which is close to the (111) lattice spacing of cubic copper. From the above analysis, it is confirmed that the hierarchical structure is a particle-on-particle Cu-Cu$_2$O heterostructure, instead of core-shell composite. The Cu particles attach on the (110) facets of Cu$_2$O truncated octahedron.
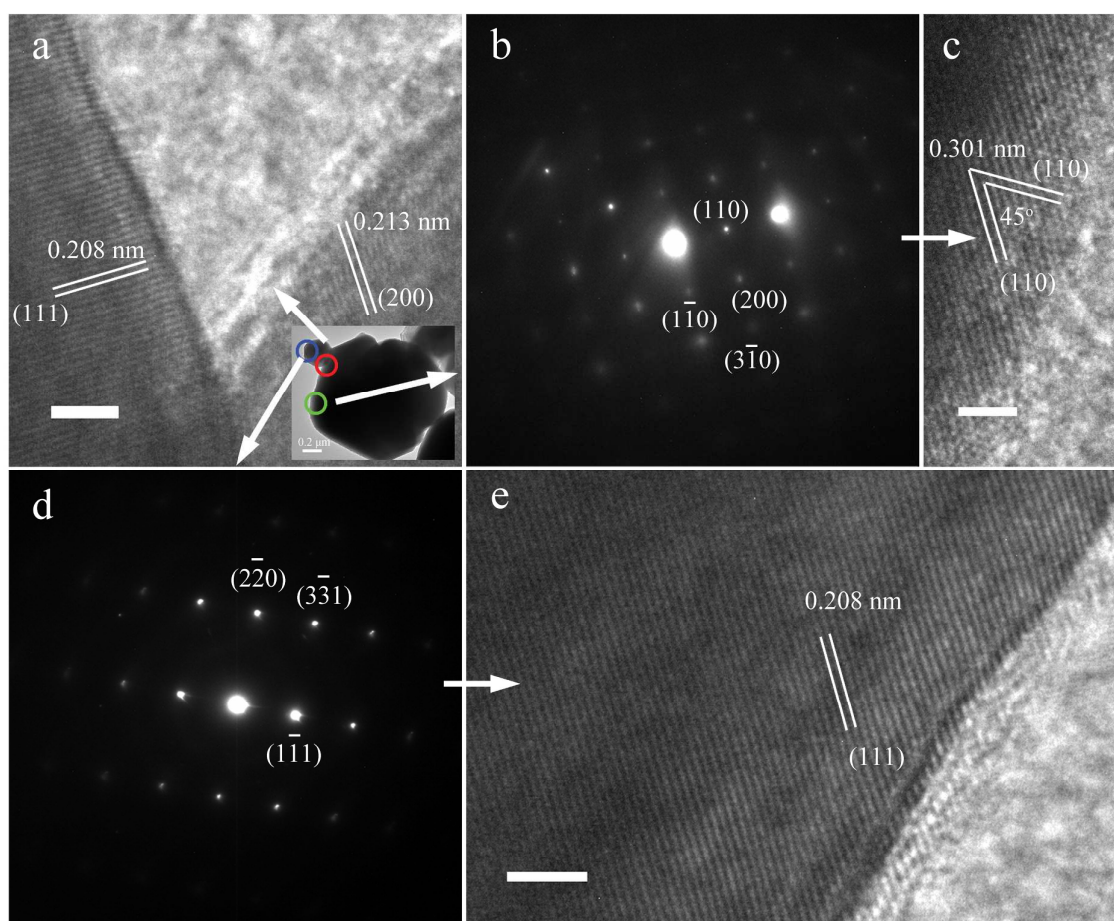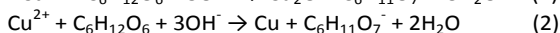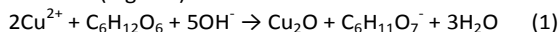

Fig. 3 Heterostructure for Cu-Cu$_2$O(60): (a) HRTEM image of the interface between the smaller particle and the larger truncated octahedron (marked with a red circle in the insert TEM image); (b) SAED pattern and (c) HRTEM of the larger truncated octahedron; (d) SAED pattern and (e) HRTEM of the smaller particle. The scale bar is 2 nm.

As described above, such a Cu-Cu$_2$O structure can be acquired by a simple hydrothermal method. How are the Cu (II) reduced to Cu(I) and Cu(0) in order, forming such a hybrid structure? It is rare in nanocrystal systems that particles spontaneously nucleate and grow in solution without a driving force such as a supersaturated solution, a strong reducing

agent, or the use of high temperature to overcome the energy barrier toward nucleation.[30] In this experiment, the reducing agent glucose under heating applies the driving force for crystallization.

It is reported that Cu^{2+} is prone to be reduced to Cu(I) transient state before it is over reduced to Cu.[31]

Thermodynamic calculations indicate that the Cu(I) species should be colourless $[Cu(OH)_2]^-$.[32] Because of the poor coordination ability of $C_6H_{12}O_6$ and $C_6H_{11}O_7^-$ compared to amine, the $[Cu(OH)_2]^-$ complex rapidly dehydrates in a alkaline solution and nucleates as Cu_2O particles.[27] Thus Cu_2O is formed in the kinetic control process following net reaction eq. (1). For example, pure Cu_2O is obtained when the reaction time is short (e.g. 1 h).

$$2Cu^{2+} + C_6H_{12}O_6 + 5OH^- \rightarrow Cu_2O + C_6H_{11}O_7^- + 3H_2O \quad (1)$$
$$Cu^{2+} + C_6H_{12}O_6 + 3OH^- \rightarrow Cu + C_6H_{11}O_7^- + 2H_2O \quad (2)$$

As OH^- is gradually consumed by prolonging the reaction, the $[OH^-]$ is not sufficient to protect the formed Cu(I) species so that the transient state of Cu(I) is easier to be further reduced to Cu in the thermodynamic control process following net reaction eq. (2). In addition, the energy barrier for nucleation of Cu is much lower by nucleating a second phase onto a seed Cu_2O truncated octahedron than by homogeneous nucleation,[30,33] Cu particles tend to nucleate on the high-energy (110) plane[34] of Cu_2O when prolonging the reaction time. As a result, the Cu-on-Cu_2O hybrid structure is formed. Interestingly, the content of Cu can be tuned by varying the reaction temperature. The amount of Cu in the composite increases with temperature because higher temperature is more conductive to the formation of thermodynamic stable product (i.e. Cu). This method can avoid any toxic reagent and is surfactant free. The glucose acts as both a green reductant and a structure-directing agent. The operating temperature can be as low as 60 ^{o}C. In addition, much potential is remained to control the size and composition of the Cu-Cu_2O hybrid material.

3.2. Electrocatalytic activity of CHT/Cu_2O/FTO, CHT/Cu-Cu_2O/FTO, and CHT/Cu/FTO

One advantage of inorganic materials is the nice dispersibility in aqueous solution.[35] The obtained material can be easily dispersed ultrasonically and drop cast onto FTO to form a modified working electrode. Here, CHT, rather than Nafion, was used to form a crosslinking net to immobilize the electrode material[36] because the former gave better performance than the latter (Fig. S1). CV experiments were carried out to measure the electrocatalytic performance of CHT/Cu-Cu_2O/FTO toward glucose oxidation in 0.1 M NaOH solution at a scan rate of 50 mV s^{-1}. In the control experiment, no peaks were observed and the current was negligible with bare FTO or CHT/FTO as the working electrode in the absence and presence of 1 mM glucose (Fig. S2). It is concluded that FTO can be a good substrate for electrochemical sensing with little background response and CHT does not affect the electrocatalytic performance of the studied electrodes. Compared to glassy carbon electrode (GCE), the FTO electrode is more versatile and cost-effective.
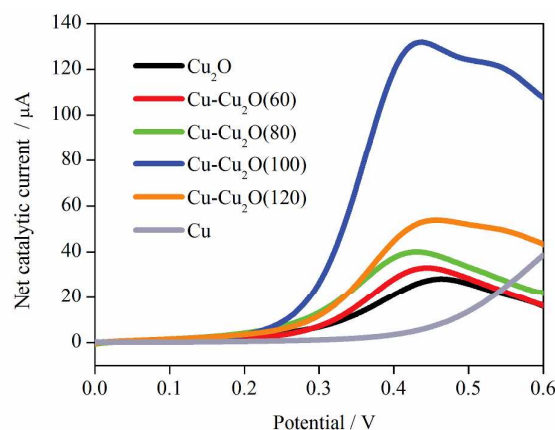

Fig. 4 Net electrocatalytic current ($\Delta I = I_{cat} - I_b$) against potential. I_b and I_{cat} are the positively scanned current from CV in the absence and presence of 1 mM glucose (Fig. S3), respectively.

Upon deposition of Cu_2O, Cu-Cu_2O or Cu on FTO, the current dramatically increased in 0.1 M NaOH solution, but no redox peaks were observed (curve a in Fig. S3). After 1 mM glucose was added into the electrolyte, an oxidation peak appeared at ~0.42 V (curve b in Fig. S3) due to the oxidation of glucose, and an obvious increase in current was observed on all modified electrodes. The possible mechanism for glucose oxidation can be explained as follows:[37] first, Cu(I) is electro-oxidized to Cu(II) and then to Cu(III) in an alkaline media. Glucose is oxidized to gluconic acid with the assistance of Cu(II)/Cu(III) redox couple. Here, the Cu(III) species are proposed to act as an electron-transfer mediator. To have a direct view of the catalytic ability, the net electrocatalytic oxidation current was obtained by subtracting the background current (I_b, Fig. S3, curve a) in the absence of glucose from the oxidation current (I_{cat}, Fig. S3, curve b) in the presence of glucose. Fig. 4 shows the net catalytic current as a function of applied potential. The net electrocatalytic oxidation current was almost zero in the potential range of 0 - 0.2 V for CHT/Cu_2O/FTO and CHT/Cu-Cu_2O/FTO electrodes, which exhibited an oxidation peak in the potential range of 0.2 – 0.6 V. However, the CHT/Cu/FTO electrode did not yield net electrocatalytic oxidation current in the potential range of 0 - 0.3 V, and the net current increased slowly from 0.3 to 0.4 V and then quickly from 0.4 to 0.6 V without an oxidation peak observed. In the potential between 0.3 and 0.5 V, the oxidation current for CHT/Cu/FTO was lower than that for CHT/Cu_2O/FTO and CHT/Cu-Cu_2O/FTO. These observations suggest that the CHT/Cu_2O/FTO and CHT/Cu-Cu_2O/FTO electrodes show higher electrocatalytic activity than the CHT/Cu/FTO electrode for electrocatalytic oxidation of glucose. As compared to the CHT/Cu_2O/FTO, the CHT/Cu-Cu_2O/FTO electrodes produce higher peak current, indicating that the hybrid structure possesses higher electrocatalytic activity. For these Cu-Cu_2O composite electrodes, the peak current first increases and then decreases with the content of Cu, and the highest peak current obtained at a Cu/Cu_2O molar ratio of 0.83 reaches 132 μA.

3.3. Cu content dependent electrocatalytic activity

The observed different electrocatalytic behavior reveals that the content of Cu has a significant influence on the performance of modified electrode because of the similar morphology but different amount of Cu. Although Cu is not an active component, the growth of copper on the Cu_2O truncated octahedron is able to increase the performance of glucose sensing. Therefore, Cu and Cu_2O must show a synergistic effect on electrocatalytic activity. It is well known that metal copper is one of the best conductors of electricity, which plays a key role in catalysis and energy storage.[38] The expected improvement of conductivity due to the presence of Cu facilitates charge transfer and hence electrocatalysis.

The EIS is an effective method for probing the electron transfer properties at the electrode/electrolyte interface. To clarify the effect of Cu in the $Cu-Cu_2O$ composite structure, the EIS was performed with a 10 mL 0.1 M KCl solution containing 5 mM $Fe(CN)_6^{3-/4-}$ as the supporting electrolyte. Fig. 5a presents Nyquist plots for the CHT/Cu/FTO, CHT/Cu-Cu_2O/FTO and CHT/Cu_2O/FTO electrodes. The EIS for the electrodes modified with Cu_2O, Cu-Cu_2O and Cu particles includes two semicircular parts and a linear part. The left semicircular part at high frequencies corresponds to the electrolyte diffusion in catalyst pores (Z_{pore}), demonstrating the porosity of the entire modified electrode. The middle semicircular part at middle frequencies corresponds to the electron transfer limited process at the electrode/electrolyte interface, and the diameter represents the electron transfer resistance (R_{ct}). The linear part at low frequencies corresponds to the diffusion process (Z_N) of electrolyte. Herein, we focus the R_{ct} of the samples to value the electron transfer ability of the electrode. As compared to the CHT/Cu_2O/FTO electrode, the CHT/Cu/FTO electrode gives much lower R_{ct} because charge transfer in the metal Cu is faster than in the Cu_2O semiconductor. When Cu particles are grown on Cu_2O to form a hybrid structure, the R_{ct} falls between the resistance values of CHT/Cu/FTO and CHT/Cu_2O/FTO. This indicates that the presence of Cu improves the interfacial charge transfer property. For the five electrodes, the R_{ct} increases with decreasing copper amount, as shown in Fig. 5b. Among these composite electrodes, the CHT/Cu-Cu_2O(120)/FTO electrode gives the lowest R_{ct}, which is comparable to that of CHT/Cu/FTO and much lower than that of CHT/Cu_2O/FTO. The above results indicate that increasing the amount of copper in the hybrid materials is favorable for the electron transfer between the electrochemical probe $Fe(CN)_6^{3-/4-}$ and the modified FTO electrode. Electron charge transfer process occurred more easily on the copper-rich surface (square in Fig. 5b).

For comparison, the relationship between oxidation peak current obtained from Fig. 4 and Cu content is also plotted in Fig. 5b (circle). Although the content of Cu_2O is decreased from pure Cu_2O to the hybrid structure, the peak current or electrocatalytic activity is enhanced because the number of effective active sites in Cu_2O is increased due to the improved conductivity. In addition, the existence of an appropriate quantity of Cu particles spaces Cu_2O particles and enlarges the exposed surface area of Cu_2O. However, when too much Cu is included in the composite electrode (e.g. CHT/Cu-Cu_2O(120)/FTO), the electrocatalytic activity on the oxidation of glucose is lessened due to the reduced amount of Cu_2O. For the extreme case, the pure Cu electrode exhibits much lower electrocatalytic activity as revealed by the low current at 0.42 V (Fig. 4). Therefore, there is an optimal ratio of Cu/Cu_2O for the best electrocatalytic activity because Cu is more conductive but less electrocatalytic active while Cu_2O is less conductive but more electrocatalytic active. As the electrocatalytic activity is positively correlated with the electrochemical active area of the electrode, the electrochemical active area of these electrodes increases gradually with the Cu amount up to a Cu/Cu_2O molar ratio of 0.83 and then decreases gradually with further increasing the Cu amount based on the above results.
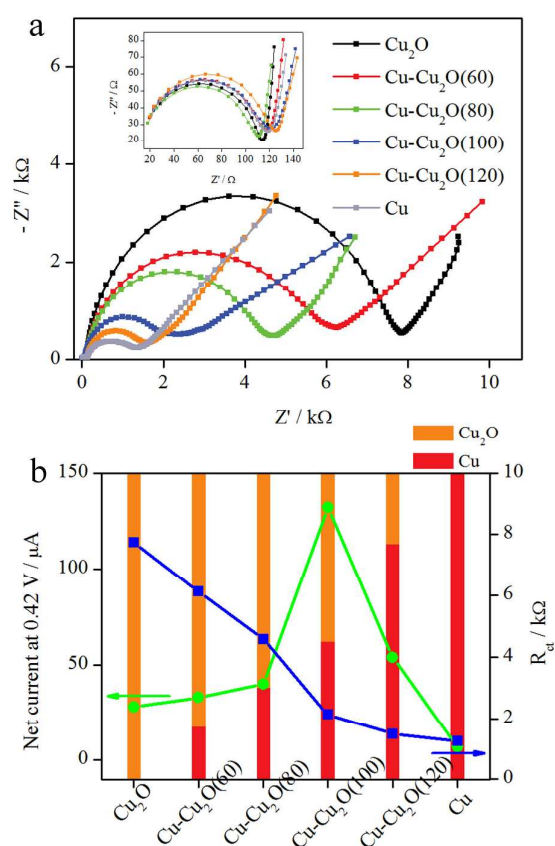

Fig. 5 (a) Nyquist plots for the CHT/Cu/FTO, CHT/Cu-Cu_2O/FTO and CHT/Cu_2O/FTO, the inset showing the enlarged part between 20 and 140 Ω; (b) effect of component on the catalytic performance and R_{ct}.

3.4. Amperometric response, selectivity, stability and reproducibility of the CHT/Cu-Cu_2O(100)/FTO towards glucose oxidation

Finally, the performance of the best CHT/Cu-Cu_2O(100)/FTO electrode was optimized by varying the amount of catalyst and

CHT. It was found that the electrode containing 0.89 mg cm^{-2} Cu-Cu$_2$O(100) and 0.022 mg cm^{-2} CHT gave the best response.

To obtain an optimal amperometric response to glucose, the effect of applied potential on the response current was investigated. Fig. 6a displays current-time curves upon successive addition of glucose (0.1 mM for each time) to the electrolyte at different applied potentials. The current increased more sharply with increasing the potential from +0.30 V to +0.60 V. However, the noise current also increased with increasing the applied potential. By comparison, potential of +0.40 V gave sharp current response but low noise current, which was thus chosen as the working potential for the following experiments.

Amperometric measurements of CHT/Cu-Cu$_2$O(100)/FTO were carried out at +0.40 V by successive injection of glucose into 0.1 M NaOH under stirring (Fig. 6b). The oxidation current reached a maximum steady-state value and achieved 95% of the steady-state current within 5 s. The dependence of current on glucose concentration is shown in Fig. 6C. The linear range of the glucose detection fell in the range of 0.01 – 2.00 mM (R^2 = 0.9938) with a slope of 55.63 µA mM^{-1} (Fig. 6c), and a sensitivity (slope/geometric area) of 618.1 µA mM^{-1} cm^{-2} was obtained (Table 1). The detection limit was estimated to be 0.74 µM at S/N (signal/noise) = 3.[39] Comparisons between this sensor and previously reported sensors for glucose are summarized in Table 1. By comparison, the CHT/Cu-Cu$_2$O(100)/FTO electrode shows advantage in the detection of glucose at low concentrations. The good linear relation in low concentrations is suitable for quantitative determination of glucose concentration in both saliva and tears. Meanwhile, the sensitivity was higher than most of the reported literature studies.
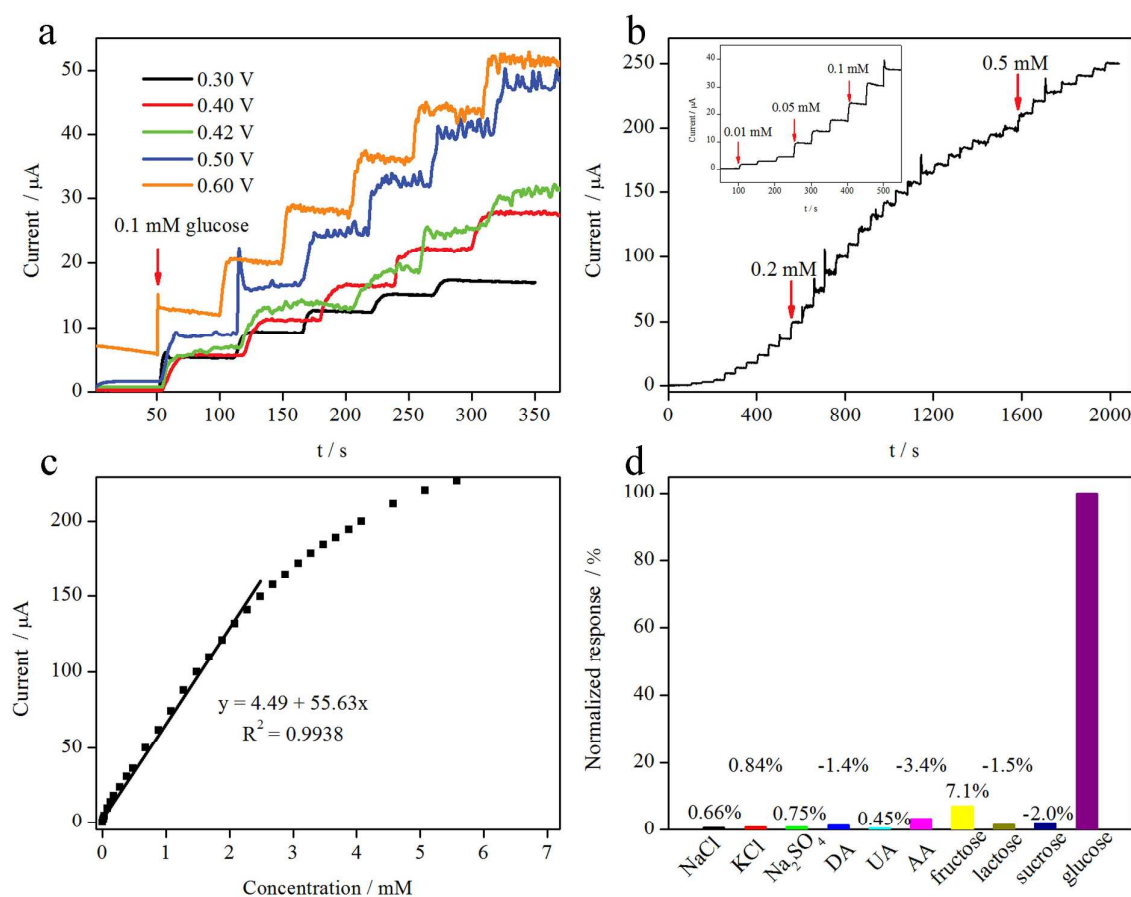

Fig. 6 (a) Current-time curves of CHT/Cu-Cu$_2$O(100)/FTO at different applied potentials with successive addition of glucose (0.1 mM for each time) to 0.1 M NaOH; (b) amperometric responses of CHT/Cu-Cu$_2$O(100)/FTO to successive injections of glucose (amount indicated with arrows in the plot) into 0.1 M NaOH at 0.40 V; (c) dependence of current at 0.4 V on glucose concentration; (d) normalized response of various interferents added to 1 mM glucose at 0.40 V.

Table 1. Comparisons between our electrode and reported nonenzymatic glucose sensors

Modified electrode	Detection potential/V	Detection limit/μM	Linear range/mM	Sensitivity/μA mM^{-1} cm^{-2}	Ref
Cu-Cu$_2$O/FTO	0.4 (*vs*. Ag/AgCl)	0.74	0.01 – 2.00	618.1*	This work
Cu/Cu$_2$O/GCE	0.45 (*vs*. SCE)	0.05	0.22 – 10.89	373.6*	11
Cu–Cu$_2$O/GCE	0.6 (*vs*. Ag/AgCl)	0.05	0.01 – 5.5	1366*	12
CQDs/Cu$_2$O/GCE	0.6 (*vs*. Ag/AgCl)	8.4	0.02 – 4.3	298	9
Cu$_2$O–Au/GCE	0.46 (*vs*. Ag/AgCl)	0.5	0.002 – 0.1	185	10

* The sensitivity was calculated by dividing slope by geometric area of electrode.

The interference of several chemicals was investigated. Fig. S4 shows the current response of the sensor to glucose and current changes after addition of NaCl, KCl, Na$_2$SO$_4$, AA, DA, UA, fructose, lactose and sucrose, respectively, which normally co-exist with glucose in the human blood serum or other samples. The used concentration of interferents is based on the fact that the normal physiological level of glucose in human blood is about 30 times that of the interfering species.[40] To compare the intensity of interference, normalized response, defined by the percentage of the current change upon addition of a chemical to the response current of glucose, is plotted in Fig. 6d. The positive sign (+) indicates an increase in current while a negative sign (-) indicates a decrease in current. For the used inorganic chemicals, the interference was small with current change less than 1% relative to the glucose response. Amperometric response of the sensor upon each addition of DA, UA, AA, lactose or sucrose was also small, with current change less than 3.5% relative to the glucose response. Among these interferents, fructose induced a larger current change, and the relative interfering response was 7.1% of the glucose signal. These results implied good selectivity of CHT/Cu-Cu$_2$O(100)/FTO.
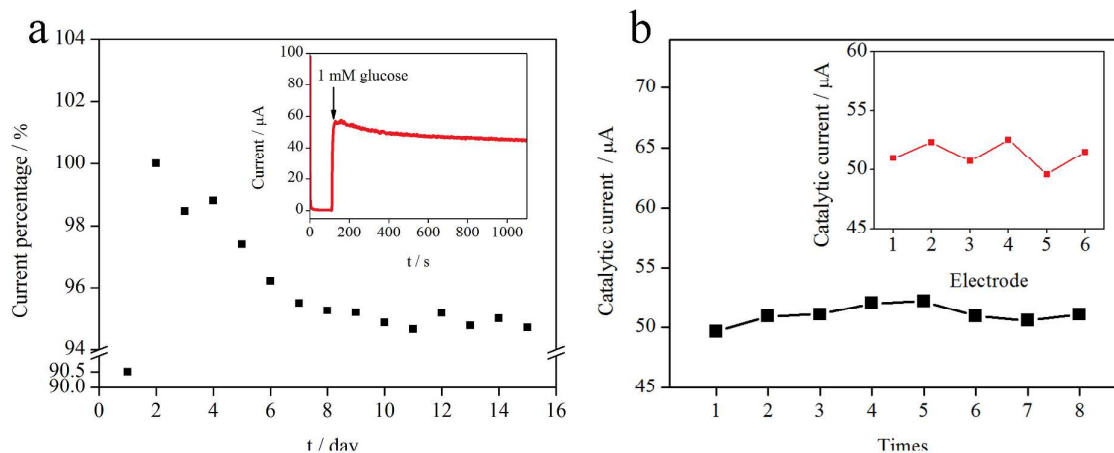

Fig. 7 (a) Stability of CHT/Cu-Cu$_2$O(100)/FTO electrode with addition of 1 mM glucose at 0.4 V. The inset shows the amperometric response of the electrode for 1 mM glucose during 1000 s; (b) the catalytic current of CHT/Cu-Cu$_2$O(100)/FTO subjected to injection of 1 mM glucose for eight times. Inset: catalytic current of six parallel CHT/Cu-Cu$_2$O(100)/FTO electrodes for detection of 1 mM glucose.

Furthermore, the stability and reproducibility of the sensor were also investigated. Fig. 7a shows the current response of the CHT/Cu-Cu$_2$O(100)/FTO electrode measured everyday in ambient conditions without special protection. The current response to 1 mM glucose decreases by 5.3% after 15 days. Shown in the inset of Fig. 7a is the current evolution with time of the CHT/Cu-Cu$_2$O(100)/FTO electrode. The current response is relatively stable up to 1000 s. CHT/Cu$_2$O/FTO and CHT/Cu/FTO electrodes also show good stability, as revealed from Fig. S5. Fig. 7b displays the current response after injection of 1 mM glucose for eight times. The current response is similar for each injection of 1 mM glucose. Six parallel CHT/Cu-Cu$_2$O(100)/FTO electrodes were fabricated to examine the reproducibility. The relative standard deviation of current response was calculated of 2.1% for the six parallel electrodes, indicating a satisfied electrode-to-electrode reproducibility. Therefore, the Cu-Cu$_2$O(100) hybrid electrode demonstrates high sensitivity, good stability and good reproducibility for glucose sensing.

4. Conclusions

In summary, Cu-Cu$_2$O hybrid truncated octahedron has been synthesized through a facile hydrothermal process. It is found that Cu$_2$O nucleates first followed by Cu growth on the high-energy (110) plane of Cu$_2$O. The existence of Cu is found to be beneficial to the electron transfer, thus enhancing the electrocatalytic activity of glucose oxidation. The content of Cu can be controlled with reaction temperature, which is able to adjust the electrochemical performance. This work would be introduced to fabricate high-sensitive and low-cost electrochemical glucose sensors.

ARTICLE

Acknowledgements

Notes and references

1   S. P. Nichols, A. Koh, W. L. Storm, J. H. Shin and M. H. Schoenfisch, *Chem. Rev.*, 2013, **113**, 2528-2549.
2   T. Choi, S. H. Kim, C. W. Lee, H. Kim, S. K. Choi, S. H. Kim, E. Kim, J. Park and H. Kim, *Biosens. Bioelectron.*, 2015, **63**, 325-330.
3   C. S. Shan, H. F. Yang, J. F. Song, D. X. Han, A. Ivaska and L. Niu, *Anal. Chem.*, 2009, **81**, 2378-2382.
4   R. Wilson and A. P. F. Turner, *Biosens. Bioelectron.*, 1992, **7**, 165-185.
5   P. Si, Y. J. Huang, T. H. Wang and J. M. Ma, *Rsc Adv.*, 2013, **3**, 3487-3502.
6   D. Jiang, Q. Liu, K. Wang, J. Qian, X. Dong, Z. Yang, X. Du and B. Qiu, *Biosens. Bioelectron.*, 2014, **54**, 273-278.
7   L. Xu, J. Xia, L. Wang, J. Qian, H. Li, K. Wang, K. Sun and M. He, *Chem. Eur. J.*, 2014, **20**, 2244-2253.
8   Y. Q. Xie and C. O. Huber, *Anal. Chem.*, 1991, **63**, 1714-1719.
9   L. Zhang, H. Li, Y. H. Ni, J. Li, K. M. Liao and G. C. Zhao, *Electrochem. Commun.*, 2009, **11**, 812-815.
10 C. L. Li, Y. Su, S. W. Zhang, X. Y. Lv, H. L. Xia and Y. J. Wang, *Biosens. Bioelectron.*, 2010, **26**, 903-907.
11 J. Luo, H. Y. Zhang, S. S. Jiang, J. Q. Jiang and X. Y. Liu, *Microchim. Acta*, 2012, **177**, 485-490.
12 Y. Zhang, B. Deng, T. R. Zhang, D. M. Gao and A. W. Xu, *J. Phys. Chem. C*, 2010, **114**, 5073-5079.
13 L. Sinatra, A. P. LaGrow, W. Peng, A. R. Kirmani, A. Amassian, H. Idriss and O. M. Bakr, *J. Catal.*, 2015, **322**, 109-117.
14 C. S. Tan, S. C. Hsu, W. H. Ke, L. J. Chen and M. H. Huang, *Nano Lett.*, 2015, **15**, 2155-2160.
15 Y. C. Li, Y. M. Zhong, Y. Y. Zhang, W. Weng and S. X. Li, *Sensor Actuat. B-chem.*, 2015, **206**, 735-743.
16 L. M. Lu, H. B. Li, F. L. Qu, X. B. Zhang, G. L. Shen and R. Q. Yu, *Biosens. Bioelectron.*, 2011, **26**, 3500-3504.
17 S. K. Vashist, D. Zheng, K. Al-Rubeaan, J. H. T. Luong and F. S. Sheu, *Biotechnol. Adv.*, 2011, **29**, 169-188.
18 J. Zhang, J. L. Ma, S. B. Zhang, W. C. Wang and Z. D. Chen, *Sensor Actuat. B-chem.*, 2015, **211**, 385-391.
19 K. Wang, Q. Liu, Q. M. Guan, J. Wu, H. N. Li and J. J. Yan, *Biosens. Bioelectron.*, 2011, **26**, 2252-2257.
20 Q. Y. Hu, F. Y. Wang, Z. Fang and X. W. Liu, *Colloid. Surface. B*, 2012, **95**, 279-283.
21 A. J. Wang, J. J. Feng, Z. H. Li, Q. C. Liao, Z. Z. Wang and J. R. Chen, *CrystEngComm*, 2012, **14**, 1289-1295.
22 Y. Zhao, Y. Li, Z. He and Z. Yan, *RSC Adv.*, 2013, **3**, 2178.
23 D. Tasis, N. Tagmatarchis, A. Bianco and M. Prato, *Chem. Rev.*, 2006, **106**, 1105-1136.
24 S. B. Kalidindi, U. Sanyal and B. R. Jagirdar, *Phys. Chem. Chem. Phys.*, 2008, **10**, 5870-5874.
25 W. Chen, Z. L. Fan and Z. P. Lai, *J. Mater. Chem. A*, 2013, **1**, 13862-13868.
26 C. J. Huang, Z. Long, M. Miyauchi and X. Q. Qiu, *CrystEngComm*, 2014, **16**, 4967-4972.
27 S. Ye, A. R. Rathmell, Y. C. Ha, A. R. Wilson and B. J. Wiley, *Small*, 2014, **10**, 1771-1778.
28 G. Wang, G. Chen, Y. Yu, X. Zhou and Y. Teng, *Rsc Adv.*, 2013, **3**, 18579-18586.
29 H. Sun, L. Zhang and Z.-S. Wang, *J. Mater. Chem. A*, 2014, **2**, 16023-16029.
30 R. Costi, A. E. Saunders and U. Banin, *Angew. Chem. Int. Ed. Engl.*, 2010, **49**, 4878-4897.
31 S. R. Ye, A. R. Rathmell, I. E. Stewart, Y. C. Ha, A. R. Wilson, Z. F. Chen and B. J. Wiley, *Chem. Commun.*, 2014, **50**, 2562-2564.
32 B. Beverskog and I. Puigdomenech, *J. Electrochem. Soc.*, 1997, **144**, 3476-3483.
33 Z. Peng and H. Yang, *Nano Today*, 2009, **4**, 143-164.
34 S. Gao, Y. F. Sun, F. C. Lei, J. W. Liu, L. Liang, T. W. Li, B. C. Pan, J. F. Zhou and Y. Xie, *Nano Energy*, 2014, **8**, 205-213.
35 N. Wang, X. Cao, X. Cai, Y. Xu and L. Guo, *Analyst.*, 2010, **135**, 2106-2110.
36 L. Ding, J. You, R. Kong and F. Qu, *Anal. Chim. Acta*, 2013, **793**, 19-25.
37 D.-L. Zhou, J.-J. Feng, L.-Y. Cai, Q.-X. Fang, J.-R. Chen and A.-J. Wang, *Electrochim. Acta*, 2014, **115**, 103-108.
38 G. Evano, N. Blanchard and M. Toumi, *Chem. Rev.*, 2008, **108**, 3054-3131.
39 H. Wu, S. Fan, W. Zhu, Z. Dai and X. Zou, *Biosens. Bioelectron.*, 2013, **41**, 589-594.
40 K. M. El Khatib and R. M. Abdel Hameed, *Biosens. Bioelectron.*, 2011, **26**, 3542-3548.